RSC Advances

PAPER

View Article Online
View Journal | View Issue

Cite this: *RSC Adv.*, 2019, **9**, 4843

Sponge-like N-doped carbon materials with Co-based nanoparticles derived from biomass as highly efficient electrocatalysts for the oxygen reduction reaction in alkaline media†

Guolong Lu,*[a] Zhiyuan Li,[a] Wenxuan Fan,[a] Mi Wang,*[ab] Shuchen Yang,[b] Jiayi Li,[a] Zhiyong Chang,[a] Hang Sun,[a] Song Liang[a] and Zhenning Liu*[a]

The development of highly efficient and low-cost catalysts towards Oxygen Reduction Reaction (ORR) is of significance for renewable energy technologies such as proton-exchange membrane fuel cells and metal–air batteries. This study is to utilize the biomass of soybean straw as the supporting carbon materials to prepare nitrogen and cobalt dual-doped porous biocarbon electrocatalysts (CoNASS) possessing high content of N (1.92%), embedding cobalt nanoparticles and sponge-like structure with high specific surface area (1185.00 m^2 g^{-1}) as well as appropriate pore diameter (~2.17 nm). Meantime, CoNASS exhibits a good electrocatalytic activity with a half-wave potential of 0.786 V (*vs.* RHE), comparable to a half-wave potential of 0.827 V (*vs.* RHE) for the commercial Pt/C. The detections of electrochemical kinetics show the electron transfer number of CoNASS is in the range of 3.84–3.92, which indicates 4-electron pathway dominantly occurs in ORR. And the limiting diffusion current density of CoNASS at 1600 rpm is around 5.8 mA cm^{-2} slightly higher than that of the benchmark Pt/C (5.6 mA cm^{-2}). This work opens a new avenue to utilize soybean straw, one of agriculture waste of large quantity, to prepare high efficient and low-cost catalysts for ORR.

Received 21st December 2018
Accepted 25th January 2019

DOI: 10.1039/c8ra10462j

rsc.li/rsc-advances

Introduction

The development of efficient, low-cost catalysts for the Oxygen Reduction Reaction (ORR) is very critical to emerging technologies for renewable energy including proton-exchange membrane fuel cells and metal–air batteries.[1–4] So far, platinum (Pt) and Pt-based catalysts are still commonly considered to exhibit excellent catalytic activities for ORR.[5,6] However, the low abundance and high cost of Pt have limited its application in ORR catalysis.[7–10] Consequently, great efforts have been devoted to exploring cost-efficient ORR catalysts as the alternative to Pt-based catalysts. Various ORR electrocatalysts containing heteroatom doped (*e.g.* Fe, Co, N and S) carbon materials have been extensively investigated and prepared in recent years, where their precursor are heteroatom-doped graphene,[11,12] carbon nanotubes,[13–15] carbon fibers,[16] polymer[17,18] as well as metal–organic framework[19] as supporting carbon materials (SCM). The performance enhancement of the abovementioned electrocatalysts is usually attributed to the inclusion of Fe or Co nanoparticles as well as N species such as pyridinic N, pyrrolic N, graphitic N and Fe/Co-N_x complex.[20–30] Nonetheless, the cost of SCM in these electrocatalysts is still relatively high and limits the practical application.

Therefore, it is desirable to develop low-cost SCM, particularly from natural biomass, for the heteroatom doping of ORR electrocatalysts.[31–34] More recently, Borghei group has shown that coconut-shell-derived and N-doped carbon materials exhibit high specific surface area (1216 m^2 g^{-1}) and good electrocatalytic activities towards ORR, which are comparable or even better than the commercial Pt/C.[35] Shao group has reported N, P co-doped porous carbon including $LaMnO_3$ nanoparticles derived from renewable natural okara is capable of excellent ORR catalysis.[36] Yet, it is still under extensive research to explore other biomass of large quantity to achieve cheaper ORR electrocatalysts with acceptable performance *via* a simpler approach.

Soybean straws are abundant renewable biomass riched in celluloses, hemicelluloses and lignin[37,38] and these contents can contribute to enhancing the activity of ORR catalysts.[39,40] To the best of our knowledge, there is no report about a facile method to synthesize ORR catalysts derived from soybean straws. Herein, the electrocatalysts (CoNASS) with N and Co co-doped spongiform porous carbon materials were prepared by a two-

[a]*Key Laboratory of Bionic Engineering (Ministry of Education), College of Biological and Agricultural Engineering, Jilin University, Changchun, Jilin Province, 130022, P. R. China. E-mail: guolonglu@jlu.edu.cn; Liu_zhenning@jlu.edu.cn*

[b]*College of Engineering, Changchun Normal University, China. E-mail: wangmi3214@126.com*

† Electronic supplementary information (ESI) available. See DOI: 10.1039/c8ra10462j

step method. The obtained CoNASS has a three-dimensional sponge-like porous structure with a high specific surface area of 1185.00 $m^2\ g^{-1}$. More importantly, the CoNASS exhibits an excellent electrocatalytic performance with a 4-electron oxygen reduction mechanism and electrocatalytic activities with ORR peak (0.81 V *vs.* RHE) in alkaline media which are comparable to those of the commercial Pt/C. The observed electrocatalytic properties of CoNASS can be attributed to the presence of pyridinic N, graphitic N and CoO nanoparticles as well as the interconnected hierarchical porous structure, which synergistically enhance electron transport and oxygen diffusion, then provide more active sites and improve ORR activity.

Experimental section

Catalyst preparation

Scheme 1 shows the process of catalyst synthesis.

Preparation of soybean straw powder (SS). Soybean straws were cleaned, purified with ethanol, and oven-dried at 80 °C for 24 h. The resulting product was grounded into powder for use.

Preparation of activated SS (ASS). SS and KOH were impregnated in deionized water at a mass ratio of 3 : 1, intensely stirred for 12 h until homo-dispersed and oven-dried at 80 °C for 72 h. The obtained uniform mixture was pyrolyzed under N_2 flow at a rate of 5 °C min^{-1} to 800 °C and kept there for 1 h.

Preparation of N-doped ASS (NASS) or N/Co co-doped material (CoNASS). ASS (20 mg) with no additives or the mixture of ASS and cobalt(II) chloride (20 mg, 2 mg), and dispersed in 20 mL of deionized water. The obtained material was filtrated, dried at 80 °C for 12 h, heated under NH_3 flow at the rate of 5 °C min^{-1} to 800 °C and kept there for 1 h. The obtained product was dispersed in 3 M HCl, washed, filtered and dried at 80 °C.

Characterization

Scanning electron microscopy (SEM) images were collected on a JEOL JSM-7500F field emission scanning electron microscope (FE-SEM). High-resolution transmission electron microscopy (HRTEM) images were obtained with a JEOL-2010 electron microscope operating at 200 kV. X-ray diffraction (XRD) was performed on a Rigaku X-ray diffractometer (D/max rA) using Cu Kα radiation at a wavelength of 1.542 Å, and the data were collected from 20° to 80°. The nitrogen adsorption–desorption isotherms were obtained on an automated gas sorption analyzer (ASAP 2020M-Physisorption Analyzer) at 77 K. The specific surface area and pore size were calculated by the Brunauer–Emmett–Teller method. Raman spectra were recorded on a laser microscope system (B&W TEK BTC 162E) with an exciting laser of 532 nm. X-ray photoelectron spectroscopy (XPS) was conducted with an ESCALAB 250Xi (Thermo Scientific).

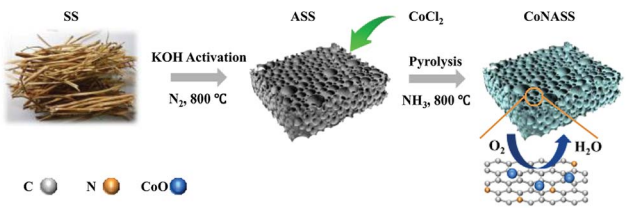

Scheme 1 Schematic diagram for the preparation of the N and Co co-doping CoNASS.

Electrochemical measurements

Electrochemical tests were evaluated on the electrochemical workstation (CHI 750E) with three-electrode cell at room temperature. Pt wire, Ag/AgCl and glassy carbon electrode were used as a counter, reference and working electrode, respectively. The working electrode slurry was prepared as follows: 5 mg catalyst and 50 μL Nafion (5 wt%, Dupont) was ultrasonically dispersed in 1 mL isopropanol and further sonicated for 1 h to form a uniform catalyst ink. Then, 15 μL of catalyst ink was deposited onto the surface of rotating ring-disk electrode (RRDE, d = 5.5 mm) and dried in air. The ORR activity was evaluated by cyclic voltammetry (CV) and linear scan voltammetry (LSV) in O_2-saturated and Ar-saturated 0.1 M KOH solution with a scan rate of 10 mV s^{-1}. The reversible hydrogen electrode (RHE) was calculated by

$$V_{RHE} = V_{Ag/AgCl} + V_{Ag/AgCl\ vs.\ NHE} + 0.059pH \quad (1)$$

The transferred electron number (n) of RRDE was expressed by

$$n = 4I_d/(I_d + I_r/N) \quad (2)$$

$$\%\ H_2O_2 = 200I_r/[N(I_d + I_r/N)] \quad (3)$$

where I_d is the disk electrode current, I_r is the ring electrode current, N = 38% is collection efficiency of the ring.

The transferred electron number (n) of RDE was analyzed by Koutecky–Levich (K–L) equations

$$j^{-1} = j_k{}^{-1} + j_l{}^{-1} = (0.035nFAC_o)^{-1} + (0.62nFAC_oD_0{}^{2/3}\nu^{-1/6}\omega^{1/2})^{-1} \quad (4)$$

where j_k is kinetic current, j_l is limiting current, F = 96486.4 C mol^{-1} is Faraday constant, $C_o = 1.2 \times 10^{-6}$ mol cm^{-3} is the concentration of O_2 in 0.1 M KOH solution, $D_o = 1.9 \times 10^{-5}$ $mol^2\ s^{-1}$ is the coefficient of O_2 in 0.1 M KOH, ω is rotation rate, A is electrode area, $\nu = 0.01$ $cm^2\ s^{-1}$ is the kinematic viscosity of the electrolyte.[41,42]

Result and discussion

The morphologies of as-prepared catalysts were characterized by SEM (Fig. 1a and b). As shown in Fig. 1a, massive structures with no obvious pores can be found on the SS surface. In contrast, hollow sponge-like structures with abundant macropores (0.5–1.5 μm) evenly distribute in CoNASS (Fig. 1b). Such a porous structure is known as a result of KOH activation during pyrolysis,[43] as described by following reactions (5)–(9).

$$6KOH + 2C = 2K_2CO_3 + 2K + 3H_2 \quad (5)$$

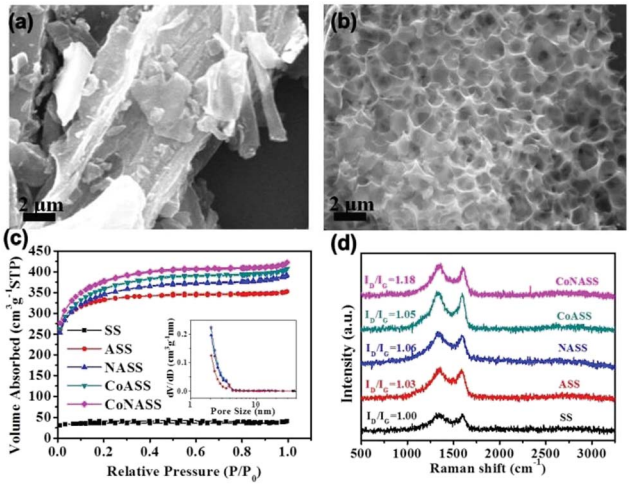

Fig. 1 SEM images of SS and CoNASS, respectively (a and b). N_2 adsorption/desorption isotherms (c) and the corresponding pore size distribution (inset). Raman spectra of CoNASS, CoASS, NASS, ASS and SS (d).

$$K_2CO_3 = K_2O + CO_2 \quad (6)$$

$$CO_2 + C = 2CO \quad (7)$$

$$K_2CO_3 + 2C = 2K + 3CO \quad (8)$$

$$C + K_2O = 2K + CO \quad (9)$$

Next, nitrogen adsorption–desorption porosimetry was conducted to further examine the porosity and specific surface area of the catalysts. As illustrated in Fig. 1c, the nitrogen adsorption–desorption isotherms (NADIs) of SS, ASS, NASS, CoASS and CoNASS represent type I isotherm with a rapid uptake under low relative pressure and a narrow hysteresis loop. It suggests the existence of numerous pores in ASS, NASS, CoASS and CoNASS, whose specific surface area/pore size is in the order: CoNASS (1185.00 $m^2\ g^{-1}$/2.17 nm) > CoASS (1132.95 $m^2\ g^{-1}$/2.19 nm) > NASS (1084.86 $m^2\ g^{-1}$/2.20 nm) > ASS (1021.40 $m^2\ g^{-1}$/2.12 nm), indicating that Co doped, N doped or Co, N dual-doped creates more pores and improves specific surface area, yet has little effects to average pore size. Together with the macropores found in SEM, it is assumed that CoNASS possesses an interconnected hierarchical porous structure, which could promote efficient mass transfer and afford good accessibility to plenty of active sites. However, the specific surface area of SS is as low as 109.81 $cm^2\ g^{-1}$, consistent with the morphology observed by SEM (Fig. 1a).

Then, the defect of as-prepared catalysts was conducted by Raman spectra (Fig. 1d). Disordered graphitic carbon and crystalline graphite correspond to the D and G bands around 1350 cm^{-1} and 1590 cm^{-1} in Raman spectra, respectively.[44,45] Therefore, the ratio of D band to G band (I_D/I_G) was calculated to evaluate the degree of defect for the pyrolyzed catalysts. The I_D/I_G ratio of SS ($I_D/I_G = 1.00$) is lower than that of ASS ($I_D/I_G = 1.03$), NASS ($I_D/I_G = 1.06$), CoASS ($I_D/I_G = 1.05$) and CoNASS ($I_D/I_G = 1.18$). These results suggest that KOH activation, Co doping, N doping or Co, N co-doping causes more defects and disorder of the catalysts, which is in line with the findings from SEM and NADIs.

TEM and HRTEM mapping were characterized to reveal the element distribution in the catalyst of CoNASS (Fig. 2). As shown in Fig. S1,† numerous nanoparticles (NPs) exists in CoASS, while no NPs were found in the TEM image of ASS, indicating Co doping could lead to producing nanoparticles after pyrolysis. In CoNASS, abundant NPs with a range size of 20–100 nm were also observed (Fig. 2c and S2†). The NPs in CoNASS were verified by lattice fringe on the HRTEM image, as the *d*-spacing of 0.245 nm corresponds to the (111) plane of the CoO. Next, XRD was conducted to be further verified the structure of NPs. As shown in Fig. S3,† the diffraction peaks of CoNASS at 36.5°, 42.4°, 61.5° and 73.7° correspond to the (111), (200), (220) and (331) planes of CoO according to the JCPDS No. 43–1004. Meantime, HRTEM element mapping images of CoNASS also show the majority of Co and O element was gathered at same place, while the doped N is evenly distributed on the carbon substrate (Fig. 2c). Together these results indicate that CoO indeed exits in catalysts of CoNASS, which could function to enhance the electron transfer and ORR performance.[46,47]

To further investigate the contents and chemical states of the elements in the as-prepared carbon samples, XPS was conducted (Fig. S4†). As summarized in Table S1,† C, N and O elements are observed in all samples. The N contents of NASS and CoNASS are 2.13% and 1.92% respectively, due to the post-treatment of chemical impregnation. It suggests the mixing with NH_3 can effectively improve the doped N content. The N species in CoNASS catalyst can be corresponding to pyridinic-N (398.2 eV), graphitic-N (401.1 eV), pyrrolic-N (399.7 eV) and oxidized-N (403.2 eV).[48,49] As shown in Fig. S4c and Table S1,† the majority of N element in CoNASS is composed of the

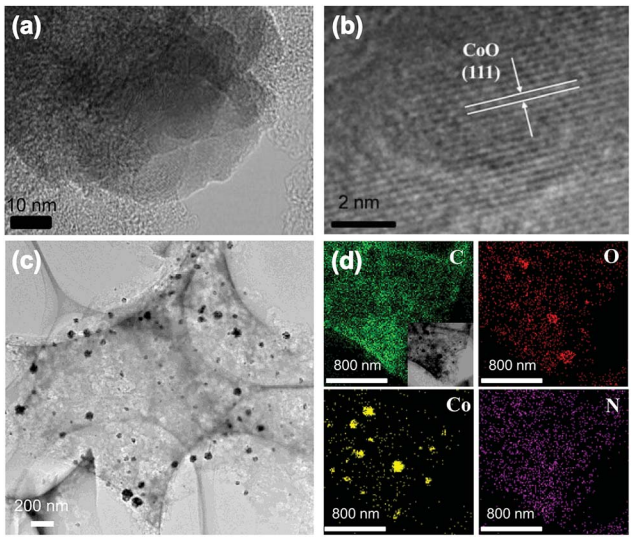

Fig. 2 TEM (a) and HRTEM images (b and c) and HRTEM element mapping of CoNASS (d).

pyridinic N and graphitic N, as well as pyrrolic N. The pyridinic N could enable adjacent carbon atoms to be active sites for O_2 adsorption and ORR initiation.[50] The graphitic-N is known as good electron-donor with good charge mobility, which could reinforce the catalytic activity of carbon *via* electron transfer and improve electrochemical performance.[51] The Co content increases from 2.30% in CoASS to 2.71% in CoNASS, which could be due to the synergistic effect of NH_3 addition and cobalt ion coordination. Meantime, as shown in Fig. S5,† the C, N and O elements also were observed in the EDS of CoNASS agreed with element mapping and XPS (Fig. 2c and S4†). The inclusion of pyridinic-N and graphitic-N, together with the embedded CoO nanoparticles, could synergistically contribute to the ORR performance of CoNASS.

To evaluate the electrocatalytic activity of the catalysts (SS, ASS, NASS, CoASS, CoNASS and Pt/C), we first performed cyclic voltammetric (CV) measurements using rotating disk electrode (RDE) with the potential range from 0.0 to 1.2 V (*vs.* RHE) in O_2- or Ar-saturated 0.1 M KOH solution at a scan rate of 10 mV s^{-1}. As control, 20 wt% Pt/C catalyst was served and compared with as-prepared catalysts, where there is a well-defined cathodic oxygen reduction peak in O_2-saturated for all as-prepared electrocatalysts, but not in Ar-saturated electrolytes. Compared with the peak potential 0.61 V of non-activited SS materials, all the activated catalysts show a more positive peak potential at 0.71 V for ASS, 0.80 V for NASS, 0.76 V for CoASS, as well as 0.81 V for CoNASS which is only slighter lower than 0.86 V for Pt/C (Fig. 3a). According to the above electrochemical results, CoNASS (N, Co co-doped) exhibits the most enhanced ORR activity than ASS (only activated), NASS (N-doped), CoASS (Co-doped), which indicates Co, N co-doped carbon materials is an efficient way to improve the activity of ORR catalysts. To gain further insight into the ORR performance of catalysts, linear scan voltammetry (LSV) measurements were conducted at 1600 rpm in O_2-saturated 0.1 M KOH solution. As shown in Fig. 3b, the ORR activity of CoNASS with E_{onset} (onset potential) 0.87 V and $E_{1/2}$ (half-wave potential) 0.79 V is only slightly lower than that of the commercial Pt/C with E_{onset} 0.94 V and $E_{1/2}$ 0.83 V, where the electrocatalysis activities of CoNASS are well agreed with that found by CV(Fig. 3a).

In order to quantify the kinetics of the ORR, LSV curves of CoNASS at different rotation speeds from 100 to 2500 rpm in O_2-saturated 0.1 M KOH solution were further tested. The LSV

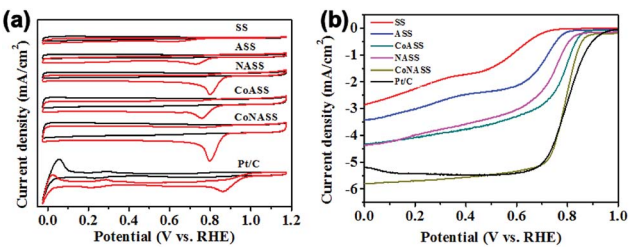

Fig. 3 CV curves of SS, ASS, NASS, CoASS, CoNASS and Pt/C in O_2- and Ar-saturated 0.1 M KOH solution (a) and LSV curves of SS, ASS, NASS, CoASS, CoNASS and Pt/C in O_2-saturated 0.1 M KOH solution at 1600 rpm (b).

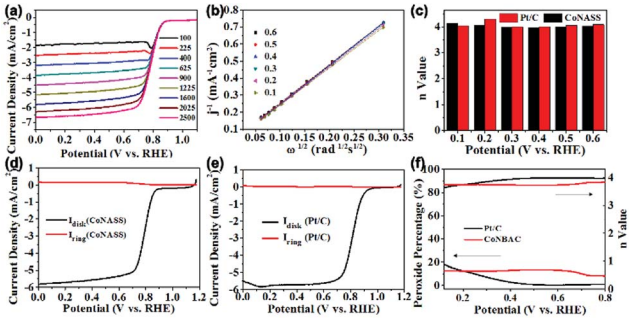

Fig. 4 The LSV curves of CoNASS at the rotation speeds of 100, 225, 400, 625, 900, 1225, 1600, 2025 and 2500 rpm (a) obtained from RDE measurements. The corresponding Koutecky–Levich (K–L) plots (b) and electron transfer numbers (*n*) of CoNASS and Pt/C (c). The LSV curves of CoNASS and Pt/C in 0.1 M KOH solution at 1600 rpm (d and e) respectively obtained from RRDE measurements. The H_2O_2 yield and *n* value of CoNASS and Pt/C calculated with eqn (2) and (3) (f).

curves shown in Fig. 4a exhibit that the limiting current density increases with increasing of rotation speed. Electron transfer number (*n*: 2-electron or 4-electron), which stands for the generation of H_2O or H_2O_2, is a major factor to evaluate ORR properties.[34] The *n* of CoNASS calculated from the slope of the K–L plots (Fig. 4b) using Koutecky–Levich (K–L) equation (eqn (2)) is 4.03 (Fig. 4c) which is closed to 4.08 for 20 wt% Pt/C (Fig. S6†), indicating the ORR mainly proceeds *via* a one-step, 4-electron ORR pathway. To verify the *n* values and peroxide yield, LSV measurements with rotating ring-disk electrode (RRDE) were performed at 1600 rpm in O_2-saturated 0.1 M KOH and the corresponding *n* values and peroxide yields were calculated according to eqn (2) and (3) (Fig. 4d). As shown in Fig. 4d–f, 4-electron reaction dominates catalysis by CoNASS (average $n = 3.75$) with low production of H_2O_2 (less than 12.14%), while Pt/C also exhibit a 4-electron pathway (average $n = 3.95$) with the production of H_2O_2 (around 5.3%), which is consistent with the results from K–L plots. These results clearly demonstrate a major four-electron transfer pathway for CoNASS as similar as that for commercial Pt/C in alkaline media.

Conclusions

In summary, N and Co dual-doped catalyst (CoNASS) utilizing biomass, *i.e.* soybean straw, as supporting carbon material was prepared, characterized and tested in alkaline media as electrocatalysts towards ORR. The electrocatalyst of CoNASS possesses an interconnected hierarchical porous structure with a high specific surface area and contains catalytically active pyridinic N and graphitic N as well as encapsulated CoO nanoparticles. Meantime, CoNASS shows more excellent ORR activities in alkaline media than that of SS (non-activation), ASS (activation), NASS (only N doped), CoASS (only Co doped), even exhibits comparable ORR activities to commercial Pt/C. The work opens a new avenue to utilize biomass to prepare high efficient and low-cost ORR electrocatalysts as an alternative to replace commercial Pt/C for potential renewable energy technologies, such as metal–air batteries and fuel cells.

Conflicts of interest

There are no conflicts of interest to declare.

Acknowledgements

This work was supported by the National Natural Science Foundation of China (51605188, 51605187, 51607010 and 21673098), Department of Education of Jilin Province (JJKH20180093KJ, JJKH20181163KJ and JJKH20180160KJ), Program for JLU Science and Technology Innovative Research Team and The Joint Program of Jilin Province and JLU (SXGJQY2017-1 and SXGJSF2017-2), Key Scientific & Technological Research & Development Projects in Jilin Province (Grant No. 20180201038GX), Jilin Province Development and Reform Commission (Grant No. 2016C029).

References

1 C. D. Liu, G. L. Li, G. C. Cheng, C. Hao, S. M. Chen and Y. Y. Xie, *RSC Adv.*, 2016, **6**, 73581–73588.
2 K. Surya, M. S. Michael and S. R. S. Prabaharan, *Solid State Ionics*, 2018, **317**, 89–96.
3 A. L. Zhu, D. P. Wilkinson, X. E. Zhang, Y. L. Xing, A. G. Rozhin and S. A. Kulinich, *Journal of Energy Storage*, 2016, **8**, 35–50.
4 P. Tan, B. Chen, H. R. Xu, H. C. Zhang, W. Z. Cai, M. Ni, M. L. Liu and Z. P. Shao, *Energy Environ. Sci.*, 2017, **10**, 2056–2080.
5 B. Fang, J. H. Kim, M. S. Kim and J. S. Yu, *Acc. Chem. Res.*, 2013, **46**, 1397–1406.
6 B. Fang, N. K. Chaudhari, M. S. Kim, J. H. Kim and J. S. Yu, *J. Am. Chem. Soc.*, 2009, **131**, 15330–15338.
7 Y. J. Wang, W. Y. Long, L. L. Wang, R. S. Yuan, A. Ignaszak, B. Z. Fang and D. P. Wilkinson, *Energy Environ. Sci.*, 2018, **11**, 258–275.
8 S. L. You, P. Luo, L. Fang, J. J. Gao, L. Liu, H. T. Xu, H. J. Zhang and Y. Wang, *Electrochim. Acta*, 2019, **294**, 406–412.
9 Y. J. Wang, N. N. Zhao, B. Z. Fang, H. Li, X. T. T. Bi and H. J. Wang, *Chem. Rev.*, 2015, **115**, 3433–3467.
10 Y. J. Wang, B. Z. Fang, H. Li, X. T. T. Bi and H. J. Wang, *Prog. Mater. Sci.*, 2016, **82**, 445–498.
11 W. M. Wu, J. G. Leng, H. L. Mei and S. B. Yang, *J. Colloid Interface Sci.*, 2018, **521**, 11–16.
12 W. Q. Kong, K. K. Yao, X. D. Duan, Z. G. Liu and J. W. Hu, *Electrochim. Acta*, 2018, **269**, 544–552.
13 J. C. Li, P. X. Hou and C. Liu, *Small*, 2017, **13**, 1702002.
14 R. Li, X. Z. Wang, Y. F. Dong, X. Pan, X. G. Liu, Z. B. Zhao and J. S. Qiu, *Carbon*, 2018, **132**, 580–588.
15 T. T. Zhao, S. Gadipelli, G. J. He, M. J. Ward, D. Do, P. Zhang and Z. X. Guo, *Chemsuschem*, 2018, **11**, 1295–1304.
16 J. L. Ma, F. L. Meng, D. Xu and X. B. Zhang, *Energy Storage Materials*, 2017, **6**, 1–8.
17 G. L. Lu, Y. L. Zhu, K. L. Xu, Y. H. Jin, Z. J. Ren, Z. N. Liu and W. Zhang, *Nanoscale*, 2015, **7**, 18271–18277.
18 G. L. Lu, H. S. Yang, Y. L. Zhu, T. Huggins, Z. J. Ren, Z. N. Liu and W. Zhang, *J. Mater. Chem. A*, 2015, **3**, 4954–4959.
19 J. Ying, J. Li, G. P. Jiang, Z. P. Cano, Z. Ma, C. Zhong, D. Su and Z. W. Chen, *Appl. Catal., B*, 2018, **225**, 496–503.
20 M. J. Liu and J. H. Li, *ACS Appl. Mater. Interfaces*, 2016, **8**, 2158–2165.
21 C. Wu, Y. H. Zhang, D. Dong, H. M. Xie and J. H. Li, *Nanoscale*, 2017, **9**, 12432–12440.
22 J. H. Shen, L. Meng, Y. Y. Liu, C. Chen, Y. H. Zhu and C. Z. Li, *RSC Adv.*, 2018, **8**, 22193–22198.
23 P. P. Gao, M. Sun, X. B. Wu, S. Z. Zhou, X. T. Deng, Z. Y. Xie, L. Xiao, L. H. Jiang and Q. Z. Huang, *RSC Adv.*, 2018, **8**, 26934–26937.
24 S. Yasuda, Y. Uchibori, M. Wakeshima, Y. Hinatsu, H. Ogawa, M. Yano and H. Asaoka, *RSC Adv.*, 2018, **8**, 37600–37605.
25 H. Liu, M. Q. Wang, Z. Y. Chen, H. Chen, M. W. Xu and S. J. Bao, *Dalton Trans.*, 2017, **46**, 15646–15650.
26 Q. J. Niu, J. X. Guo, Y. H. Tang, X. D. Guo, J. Nie and G. P. Ma, *Electrochim. Acta*, 2017, **255**, 72–82.
27 J. C. Carrillo-Rodriguez, I. L. Alonso-Lemus, A. A. Siller-Ceniceros, E. Martinez, P. Piza-Ruiz, G. Vargas-Gutierrez and F. J. Rodriguez-Varela, *Int. J. Hydrogen Energy*, 2017, **42**, 30383–30388.
28 Y. J. Wang, B. Z. Fang, X. M. Wang, A. Ignaszak, Y. Y. Liu, A. J. Li, L. Zhang and J. J. Zhang, *Prog. Mater. Sci.*, 2018, **98**, 108–167.
29 M. Sun, D. Davenport, H. J. Liu, J. H. Qu, M. Elimelech and J. H. Li, *J. Mater. Chem. A*, 2018, **6**, 2527–2539.
30 G. Zhang, G. C. Wang, H. J. Liu, J. H. Qu and J. H. Li, *Nano Energy*, 2018, **43**, 359–367.
31 H. Feng, H. Hu, H. Dong, Y. Xiao, Y. Cai, B. Lei, Y. Liu and M. Zheng, *J. Power Sources*, 2016, **302**, 164–173.
32 M. Chen, S. Jiang, C. Huang, X. Wang, S. Cai, K. Xiang, Y. Zhang and J. Xue, *Chemsuschem*, 2017, **10**, 1803–1812.
33 M. Zhang, X. Jin, L. Wang, M. Sun, Y. Tang, Y. Chen, Y. Sun, X. Yang and P. Wan, *Appl. Surf. Sci.*, 2017, **411**, 251–260.
34 Y. Lu, N. Zhu, F. Yin, T. Yang, P. Wu, Z. Dang, M. Liu and X. Wei, *Biosens. Bioelectron.*, 2017, **98**, 350.
35 M. Borghei, N. Laocharoen, E. Kibena-Poldsepp, L. S. Johansson, J. Campbell, E. Kauppinen, K. Tammeveski and O. J. Rojas, *Appl. Catal., B*, 2017, **204**, 394–402.
36 J. Hu, Z. W. Shi, C. Su, B. Q. Lu, Z. P. Shao and H. Huang, *Electrochim. Acta*, 2018, **274**, 40–48.
37 M. Martelli-Tosi, O. B. G. Assis, N. C. Silva, B. S. Esposto, M. A. Martins and D. R. Tapia-Blácido, *Carbohydr. Polym.*, 2017, **157**, 512–520.
38 M. Martelli-Tosi, M. d. S. Torricillas, M. A. Martins, O. Benedito Garrido de Assis and D. Rita Tapia-Blácido, *J. Nanomater.*, 2016, **2016**, 10.
39 B. Yao, P. Kolla, R. Koodali, Y. C. Ding, S. Balaranjan, S. Shrestha and A. Smirnova, *New J. Chem.*, 2017, **41**, 958–964.
40 Y. Lu, G. C. Ye, X. L. She, S. Q. Wang, D. J. Yang and Y. F. Yin, *ACS Sustainable Chem. Eng.*, 2017, **5**, 8729–8737.

41 F. P. Hu, X. G. Zhang, X. Fang and J. Zhang, *Carbon*, 2005, **43**, 2931–2936.
42 Z. Kačarević-Popović, *Energy*, 2016, **101**, 79–90.
43 J. C. Wang and S. Kaskel, *J. Mater. Chem.*, 2012, **22**, 23710–23725.
44 H. N. Yang, D. C. Lee, K. W. Park and W. J. Kim, *Energy*, 2015, **89**, 500–510.
45 Q. H. Wei, H. L. Fan, F. F. Qin, Q. X. Ma and W. Z. Shen, *Carbon*, 2018, **133**, 6–13.
46 G. H. Wang, Y. J. Deng, J. N. Yu, L. Zheng, L. Du, H. Y. Song and S. J. Liao, *ACS Appl. Mater. Interfaces*, 2017, **9**, 32168–32178.
47 X. L. Zhang, J. G. Lin, S. M. Chen, J. Yang, L. Song, X. J. Wu and H. X. Xu, *ACS Appl. Mater. Interfaces*, 2017, **9**, 38499–38506.
48 Y. Chang, C. H. Yuan, C. Liu, J. Mao, Y. T. Li, H. Y. Wu, Y. Z. Wu, Y. T. Xu, B. R. Zeng and L. Z. Dai, *J. Power Sources*, 2017, **365**, 354–361.
49 C. Hu, Y. Zhou, R. G. Ma, Q. Liu and J. C. Wang, *J. Power Sources*, 2017, **345**, 120–130.
50 D. H. Guo, R. Shibuya, C. Akiba, S. Saji, T. Kondo and J. Nakamura, *Science*, 2016, **351**, 361–365.
51 Y. J. Li, G. L. Wang, T. Wei, Z. J. Fan and P. Yan, *Nano Energy*, 2016, **19**, 165–175.